ELSEVIER

Journal of Power Sources 103 (2001) 98–112

JOURNAL OF POWER SOURCES

www.elsevier.com/locate/jpowsour

Non-intrusive measurement of the state-of-charge of lead-acid batteries using wire-wound coils

Ian R. Hill[a,*], Ed E. Andrukaitis[b]

[a]*Institute for Chemical Processes and Environmental Technology, National Research Council of Canada, Ottawa, Ont., Canada K1A 0R6*
[b]*Defence Research and Development Branch, National Defence Headquarters, 305 Rideau Street, Ottawa, Ont., Canada K1A 0K2*

Received 16 April 2001; accepted 8 June 2001

Abstract

Non-intrusive monitoring of the state-of-charge (SOC) of lead-acid batteries by the use of wire wound coils is described. Coils were attached to the outside case of the battery, adjacent to the negative end plate, and excited using ac current of frequency in the range of 1–40 kHz. The change in inductance of the coils was monitored during battery cycling, as the metallic content of the electrode changed. Following correction for temperature changes, the technique is capable of estimating the SOC of a battery to an accuracy of ±10%. The inductance profiles that were obtained changed shape as the batteries aged and also with the exciting frequency. The origins of these changes are discussed.

Keywords: Lead-acid; State-of-charge; Inductance; Coil

1. Introduction

The state-of-charge (SOC) of lead-acid batteries is of particular interest in applications that involve deep discharging, such as electric vehicles and submarine propulsion. Traditionally, the SOC is estimated from the discharging voltage and current of the battery using algorithms, or from using sensors inside the battery. However, a reliable way of probing the SOC external to the battery would be preferable. Several patents have been published during recent years concerning the use of wire-wound coils to monitor the SOC of lead-acid batteries [1–3]. With this technique, a coil is firmly attached to the battery case such that its windings are parallel to the surface of the end plate of the battery. The two end plates of a lead-acid battery are normally both the negative, metallic lead electrodes. When an ac current is applied to the coil, it generates a magnetic field that propagates along the axis of the coil winding into the battery. This alternating magnetic field can propagate through an insulator but will be absorbed by a conductor, such as a metal electrode. The energy lost to the conductor, by the magnetic field of the coil, can be detected from the drop in inductance of the coil compared with that measured in air. The alternating magnetic field generates eddy currents in the conductor that mirror the current flow in the coil and which set up an opposing alternating magnetic field. In this way, the intrinsic inductance of the coil is reduced in the proximity of the metal electrode — the coil is being used as a metal detector. This technique should be considered for applications with rechargeable batteries that have relatively flat discharge curves and especially for sealed or gelled-electrolyte systems.

During discharging of a lead-acid battery, the lead in the negative electrode active material is converted to lead sulphate, so the total metallic content of the electrode is lowered. The alternating magnetic field does not interact with lead sulphate, so the coil inductance changes with the SOC of the negative electrode. The positive electrode active material changes from lead dioxide to lead sulphate during discharging, so this electrode will not affect the coil inductance during cycling. Lead dioxide is a semiconductor and its resistance is too high to support eddy currents (91 MΩ cm at 20°C). This technique requires equipment sensitive enough to detect small changes in the coil inductance during battery cycling. The coil needs to be as close as possible to the electrode and only a small range of frequencies has been found to be useful (details of this will be given later). The changes in inductance are not quantitative by themselves because the distance between the coil and the lead electrode is not known. Rather, the battery needs to be cycled in order to generate a calibration curve relating the inductance changes to the true SOC. Because the coil is being used to detect metal, it is apparent that the batteries being

* Corresponding author. Tel.: +1-613-996-6814; fax: +1-613-991-2384.
E-mail address: ian.hill@nrc.ca (I.R. Hill).

0378-7753/01/$ – see front matter
PII: S0378-7753(01)00852-7

considered here should have non-metallic cases. This coil technique is a new application of eddy current analysis, which is in widespread use in the aerospace industry for detecting cracks or corrosion in the metal skin of aircraft. However, in the present application, the coils being used have a much larger diameter, in order to sense the average composition of the electrode.

In the first patent that was issued to Stevenson on battery monitoring using coils [1], a commercial proximity sensor was used that was operated in the frequency range of 75–135 kHz, which was the resonance region of the coil. The SOC was monitored via a shift in the resonance frequency of the coil. The patent also suggested operation of the coil at a fixed frequency. Limuti et al. [2] proposed the use of coils and capacitors for a battery monitoring system that measured SOC, electrolyte level, internal resistance and temperature. In this case, the SOC sensing coil was wrapped around the entire battery, which was not an ideal arrangement. A later patent from Beutler et al. [3] suggested using coils parallel to the end plate of a lead acid battery to measure the SOC. Here, two sizes of coil were described. The first was several large loops, whose diameter approached the dimensions of the electrode. The second was a smaller coil of about 4 cm diameter with many windings, that was positioned over the centre of the end plate. The small coil was held in a ferrite pot core, which enhanced the magnetic field of the coil and also shielded it from electromagnetic interference. The SOC of the battery was determined using both the real (resistance, R) and imaginary (inductive reactance, X_L) components of the electrical complex impedance ($Z = R + jX_L$, where $X_L = 2\pi fL$ and L is inductance). A fixed frequency was used to estimate the SOC, as above, but the use of several frequencies allowed calculation of the permeability and conductivity of the electrode sheet; from this, a more accurate SOC could be determined. Beutler et al. [3] also described measurement of the interaction between the coil and the electrolytes in the absence of electrode plates. Measurements were made on pure water and concentrated sulphuric acid (for lead-acid). The resistance (rather than inductance) of the coil was found to roughly correlate with the specific conductance of the electrolyte but the change was much lower than that arising from the metal electrodes during cycling.

The real resistive component of the impedance is a measure of energy losses in the metal, because the eddy currents represent a resistive load. This causes the resistance of the coil to increase. The imaginary inductive reactive component is related to the energy stored in the magnetic field of the coil. Consequently, the eddy currents cause the inductive reactance to fall in magnitude. The system can be modelled as two mutually interacting coils, separated by a distance that varies with the frequency, or skin depth (see Section 3.1). The present work was carried out in order to determine whether this inductance technique could be an accurate and reliable way of monitoring the SOC of a lead-acid battery throughout its useful life, plus to try and understand the finer details of the inductance profiles observed during long-term cycling. One aspect that was not addressed in any of the patents was the effect that temperature had on the inductance measurements. There is an appreciable dependence of eddy current interactions on temperature and the temperature inside a battery varies during cycling, even if the ambient temperature does not, so that is one issue addressed in the present communication.

2. Experimental

The coils used in this work were 35 mm in diameter and were hand wound onto polycarbonate spools using either 24 or 34 gauge lacquered copper wire. The ferrite pot cores and polycarbonate spools were obtained from ELNA Ferrite Labs, Inc., Woodstock, New York. The ferrite cores were made from a mixed MnZn or NiZn ferrite and had initial permeabilities of $2300 \pm 20\%$, with on optimum frequency range below 300 kHz. The coils typically had an inductance of approximately 30 mH, which increased to 120 mH when placed inside the pot core. The pot core coils had a resonance frequency in the region of 70–80 kHz, but the frequencies used in these experiments were all below that region. Impedance data were acquired using a Hewlett-Packard HP 4192A LF Impedance Analyser, which has an oscillator level in the range of 5 mV to 1.1 V. Inductance (L) was measured as (inductive reactance)/(angular frequency), or X_L/ω. Lead-acid RV batteries of 12 V were cycled using a Kikusui PBX 2020 bipolar power supply and 12 V military SLI truck batteries (6TL made by Exide Corp. and 6TLFP made by East Penn Manufacturing Co.) were cycled on a Digatron Electronic Universal Battery Tester (UBT1-50). Measurements were taken every 5 min during battery cycling using a controlling programme written using Labview 4.0. The internal temperature of the end cell being monitored by the attached coil was sampled using a thermocouple encased in a thin-walled glass tube. Voltages and currents were measured using Fluke 8840A and Hewlett-Packard 3457A multimeters. A Thermotron S-8 environmental chamber was used to equilibrate the batteries at different temperatures.

3. Results and discussion

3.1. Frequency of the ac current

Preliminary work with the coils was carried out using lead blocks and lead foil. This work established that frequencies in the range of 5–20 kHz were the most sensitive to the variation in thickness of the lead and yielded data with the best signal-to-noise ratio. The use of multiple layers of 0.075 mm lead foil in this frequency range showed that the inductance change increased in a smooth way as the total

thickness of lead increased, up to a limit beyond which increasing of thickness had little effect. This limit arises because the electromagnetic field is absorbed exponentially with penetration depth into a metal. The limiting thickness observed for the lead foil was approximately 1.65 mm at 5 kHz and 0.825 mm at 20 kHz. These thicknesses are comparable with those of the electrodes in SLI and traction lead-acid batteries. However, the electrodes in such batteries are highly porous so their interaction with the alternating magnetic field will be complex, and also superimposed with the signal from the supporting lead grid. Absorption of the electromagnetic field by the metal follows the relationship $\delta = (\pi\mu\sigma f)^{-1/2}$, where δ represents the depth at which the field is attenuated by 1/e, or 63%, and is termed as the skin depth, μ is the permeability of the material (which is equal to $4\pi \times 10^7$ H m^{-1} for non-ferromagnetic materials such as lead), σ the conductivity and f the frequency of the oscillating field. For lead, the skin depth was calculated to be 29 mm at 60 Hz, 7.3 mm at 1 kHz, 2.3 mm at 10 kHz, and 0.73 mm at 100 kHz. Using the information obtained from these preliminary studies, experiments were then carried out on commercial batteries, using frequencies in the range of 1–40 kHz.

3.2. Inductance behaviour during early cycles and the correction for battery temperature

The majority of experiments were carried out using 12 V military truck, SLI/deep cycle hybrid batteries. These were normally charged for 18 h, with a voltage limit of 14.4 V (6TL batteries with antimony alloy grids) or 15.0 V (6TLFP batteries with calcium alloy grids), with the current limited to 25 A. Following a 1 h rest, the batteries were normally discharged at 9 A, which corresponded with a reserve capacity application in the Canadian Land Forces. For consistency, the majority of the data presented here are from the same 6TL battery. Fig. 1A shows a section of the voltage and absolute current profiles during cycling and Fig. 1B shows the corresponding changes in the attached pot-core coil inductance at 10 kHz. Notice that the inductance rises during discharging and falls during charging. The inductance only changes by about 0.7% during cycling, showing that sensitive and stable instrumentation is necessary. Measurements were taken every 5 min and the data presented are the average of 10 measurements (averaged by the HP4192A). Clearly, signal averaging can be used to improve the signal-to-noise ratio. The inductance of this pot-core coil was 120.41 mH in air, which fell to 117–118 mH when it was attached to the battery. Therefore, the inductance is lower in the presence of the lead and during discharging, when lead is converted to non-metallic lead sulphate, the inductance rises. Discharging was carried out at a constant current of 9 A and it can be seen that the inductance change is almost linear with the charge withdrawn, indicating the feasibility of using these measurements to monitor the SOC of a lead-acid battery. The charging portion of Fig. 1B is of a very different shape because the initial charging current was 25 A, which tapered off when the battery voltage reached 14.4 V. Hence the rapid fall in inductance at shorter times, followed by an extensive wing. Fig. 1C is a replot of the same cycle as in Fig. 1B, but with the time axis replaced by the integrated absolute charge passed during that cycle. It can be seen that the charging and discharging portions in the figure are quite different. This will be discussed further in a later section. Because the initial charging current was 25 A, there are few data points between 100 and 160 Ah in Fig. 1C.

The lead-acid battery charging reaction is mildly exothermic and results in only a minor increase in temperature at low charging rates. With high charging rates, resistive heating and polarisation heating become important. It was expected that the inductance change would be sensitive to temperature, but it was not known how significant the effect would be relative to that from the SOC. Therefore, the pot-core coil and a lead block were placed in an environmental chamber and the inductance signal from the lead was measured at 10 kHz at several temperatures. The pot-core coil itself exhibited negligible inductance change with temperature, but the signal from the lead did change with temperature. The inductance signal tracked the change in temperature indicating that the eddy currents were stronger at lower temperature and that the resistance of the lead was important. The inductance of the pot-core coil in air at 10 kHz was 120.4 mH, which fell to 92.2 mH on the lead block at 21°C. At −24.9°C, the inductance had fallen to 86.4 mH and the linear relationship between the inductance change and the temperature yielded a proportionality factor of 0.126 mH °C^{-1}. This factor will vary with the spacing between the coil and the metal so a better way of expressing the change is as a percentage relative to the difference between the signal on lead and in air. In the present case, this was $0.126/(120.41 - 92.20) \times 100 = 0.45\%$ °C^{-1}. The temperature correction factor varied slightly with frequency because of the different skin depths involved.

The temperature dependence experiment was repeated using the same coil with a lead-acid battery and the data are plotted in Fig. 2A for 10 kHz. Again, the inductance change tracked the temperature change, so a proportionality factor could be calculated. This was 0.0311 mH °C^{-1}. As a percentage change, this was $0.0311/(120.41 - 113.73) \times 100 = 0.47\%$ °C^{-1}. The small difference between the values for the lead block and for the battery electrode show that the correction factors are consistent. The lowest trace in Fig. 2B shows the temperature variation of a 6TL battery during the some early cycles (14–17). The main temperature change occurs during the 25 A portion of charging, as expected. The total temperature increase during a cycle was approximately 7°C and the corrected and uncorrected inductance curves for 10 kHz are compared in the upper portion of Fig. 2B. The corrections to the inductance during discharging were small and arose from residual heat from the charging half-cycle. For charging, the temperature correction had the effect of

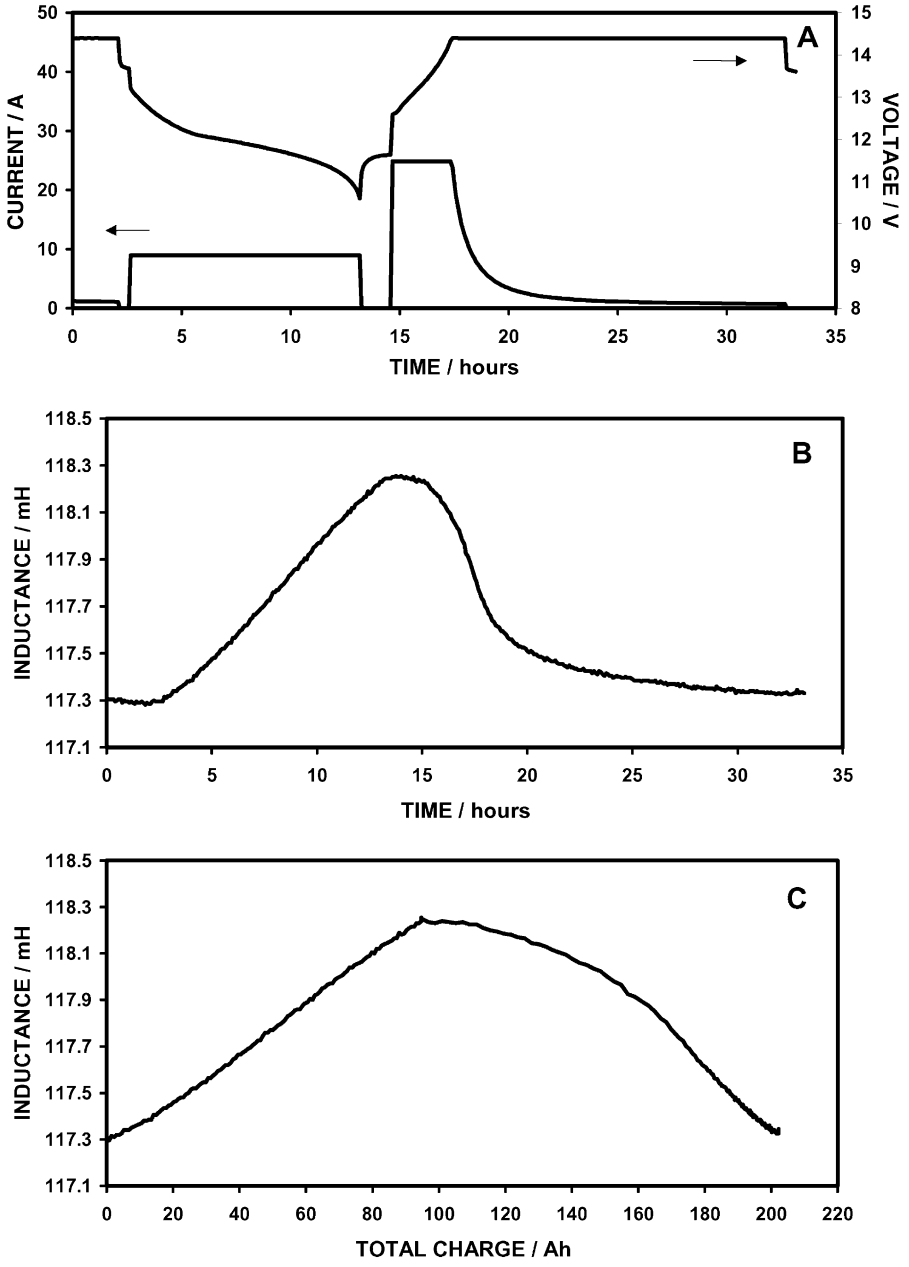

Fig. 1. One cycle of a 12 V, 6TL lead acid battery, discharged at 9 A to 10.5 V and charged using 25 A/14.4 V for 18 h: (A) Current (absolute values) and voltage profiles; (B) Inductance profile plotted against time (10 kHz); (C) Inductance profile plotted against the total absolute value of the charge passed.

flattening out the inductance plot near the end of charging. When the negative electrode is fully charged, the inductance should remain constant. The data in Fig. 2B indicate that the electrode being monitored was close to being fully charged. The battery was being charged to 110% of capacity, but an increased charging time would have been beneficial (110–120% is normally recommended). Therefore, one application of these inductance measurements can be to determine the end-of-charge of a sealed battery. In such a case, the temperature probe would need to be adjacent to the coil rather than inside the cell, as was used here. More specifically, the inductance technique will determine the end-of-charge of the negative end plate of a cell. In the present work, only one coil was used per 12 V battery, so a faulty cell elsewhere in the battery would not be detected using inductance data alone. For a 12 V battery, four of the six cells could be monitored using coils. For a large submarine cell (150 cm × 40 cm × 40 cm), which may have concentration gradients from the top to the bottom of a cell, several coils could be placed in different locations in order to determine the uniformity of negative plate discharging reactions.

Fig. 3 shows the inductance changes at 10 kHz for a defective, 14 Ah, flooded RV lead-acid battery that was going into thermal runaway during charging. This battery was charged for 15 h at 1 A, with a 14.8 V limit. However, the voltage stabilised at only 14.7 V after 12 h and the

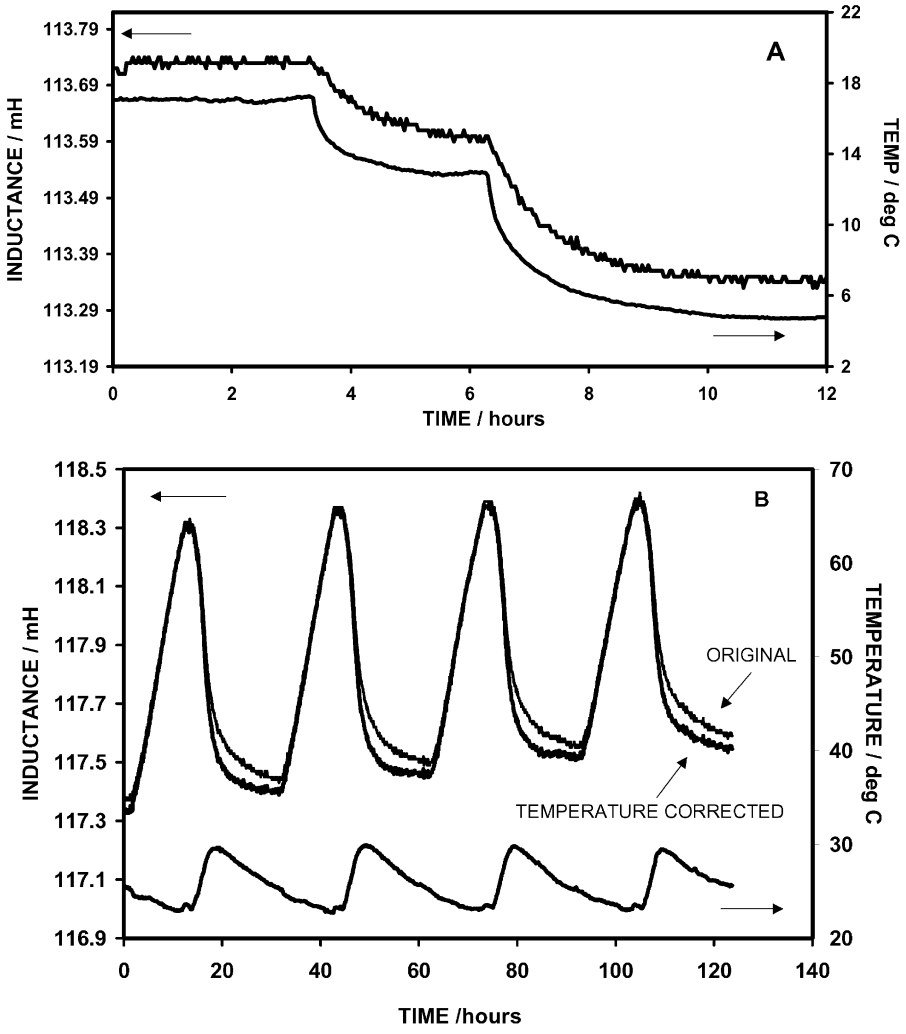

Fig. 2. (A) Inductance (10 kHz) and battery temperature changes for a RV battery being held in an environmental chamber at three set temperatures. The inductance change is linear with the temperature; (B) Inductance profiles before and after correction for battery internal temperature changes.

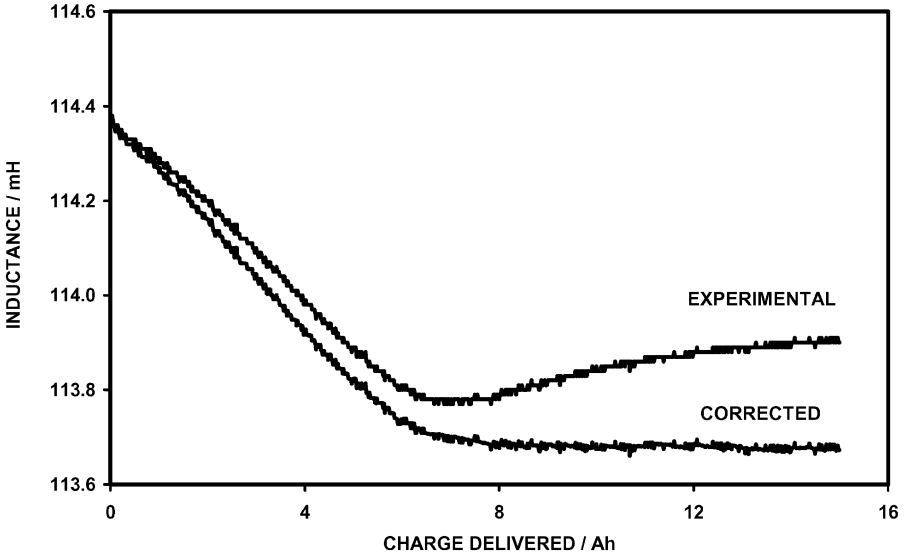

Fig. 3. Temperature correction applied to the inductance (10 kHz) of a defective 12 V, RV lead-acid battery that was being charged at 1 A/14.8 V.

temperature had climbed from 22 to 31°C by the end of charging. The experimental inductance change can be seen to be exhibiting an anomalous behaviour near the end of charging, where it begins to increase again. After correcting the data for the change in temperature, as previously described, the inductance change became flat in this region. This showed that the negative electrode had reached its maximum attainable charge after only 8 h and that further charging current was leading to gassing and heat production. Therefore, a battery monitoring system could include inductance data to detect the end-of-charge of the negative electrode, or faults associated with that electrode, including self-discharging at open circuit.

3.3. Drifting of the background inductance signal during early cycles

It will be noticed that the whole inductance plot in Fig. 2B is drifting to higher inductance values with time. This behaviour was also observed with other lead-acid batteries studied in this work and occurred during the first 20–30 cycles, after which the plots tended to be level. This rising background was seen for all of the frequencies sampled (1–40 kHz) and the magnitude of the increase correlated with the magnitude of the inductance change during one cycle, for each frequency. From this, it was apparent that the rising background involved changes to the lead electrode and did not originate from an instability of the coil-battery combination. Lead acid batteries are known take about 25 cycles for the electrode structures to stabilise [4,5]. During early cycles, the porosity of the electrodes increases, with an accompanying increase in surface area and an increase in discharge capacity for low rates. In particular, Pavlov et al. have shown how the use of expanders leads to the negative electrode active mass becoming more porous during early cycles and that the electrode swells [5]. One important factor involved in these structural changes must be the increase in molar volume by 2.64 times, when lead is oxidised to the sulphate. The rising background observed in the inductance plots in this work must be attributable to the same structural changes during early cycles. The increase in inductance corresponds to a drop in eddy current flux. This, in turn, correlates with an increase in porosity of the negative electrode, which would make the path of the eddy currents more tortuous through the complex skeletal structure of the active material, and result in a higher resistance. On the other hand, any swelling of the electrode towards the coil would result in a stronger interaction with the coil and higher magnitude inductance changes, resulting in a lower background. Because this was not observed we must assume that porosity changes are more important during these early cycles.

3.4. State-of-charge measurements

Fig. 4A shows the inductance data at 10 kHz for ten cycles of the same 6TL battery (cycles 37–46) after the background inductance signal had stopped drifting upwards. Here, charging was carried out for 14 h and approximately 110% of the previous discharge capacity was returned to the battery. The discharge capacities have been included in Fig. 4A, above the curves, and are seen to be relatively constant. The data in Fig. 4A are not exactly reproducible from cycle to cycle and do not completely correlate with the capacity. There is still slight shifting of the background inductance with time, which means that a SOC monitoring system making use of this technique would need to be recalibrated approximately every 10 deep discharges in order to maintain accuracy. Nevertheless, data from one cycle in Fig. 4A could be used to estimate the SOC during the other cycles in Fig. 4A, to an error of approximately ±10%. However, knowing the inductance at the beginning of a particular discharge enables a better estimate of the SOC, because the drifting problem is then minimised. Fig. 4B is a plot of the ratio of the (inductance change during discharging)/(capacity), for each discharge of the cycles shown in Fig. 4A. This ratio is ideally constant, but the observed scatter in the data indicates that the SOC could be estimated to an error of approximately ±7%. Of course, there are also large errors in estimating the SOC of lead-acid batteries using other techniques, such as specific gravity or discharge voltage-current measurements. An advantage of the present technique is that it can be used with gelled-electrolyte batteries. Additionally, the inductance technique can also be used when the battery is in open circuit, unlike the case for discharging voltage/current algorithms. For a gelled battery that previously had a coil attached to it and its inductance calibrated, this technique may be the best method of non-intrusively estimating the SOC. Work using gelled-electrolyte batteries is currently underway and these give similar inductance profiles to flooded batteries, as expected.

Fig. 5A shows the inductance data at 10 kHz for further cycles of the same 6TL battery (cycles 76–86) under non-ideal charging conditions; the charging time was reduced to 8 h so that the battery was slightly undercharged. Without a full recharge, the measured capacities in Fig. 5A are not as constant as those in Fig. 4A and the inductance plots are not as reproducible. For this data, the error in using one of these cycles to estimate the SOC in the other cycles is approximately ±20%. The ratio of the (inductance change during discharging)/(capacity) (Fig. 5B) is not as constant for these cycles and the error involved in estimating the SOC, when the inductance value at the beginning of discharging is known, is approximately ±12%. At the cycle 9 of Fig. 5A, an extended recharge time of 25 h was applied and the capacity recovered from 79.0 to 104.2 Ah. The inductance plot during the extended recharging continued to fall for most of the 25 h period, showing that $PbSO_4$ at the negative electrode continued to be reduced. Therefore, the inductance technique would be useful for monitoring the end-of-charge of the negative electrodes in gelled cell batteries during reconditioning charges.

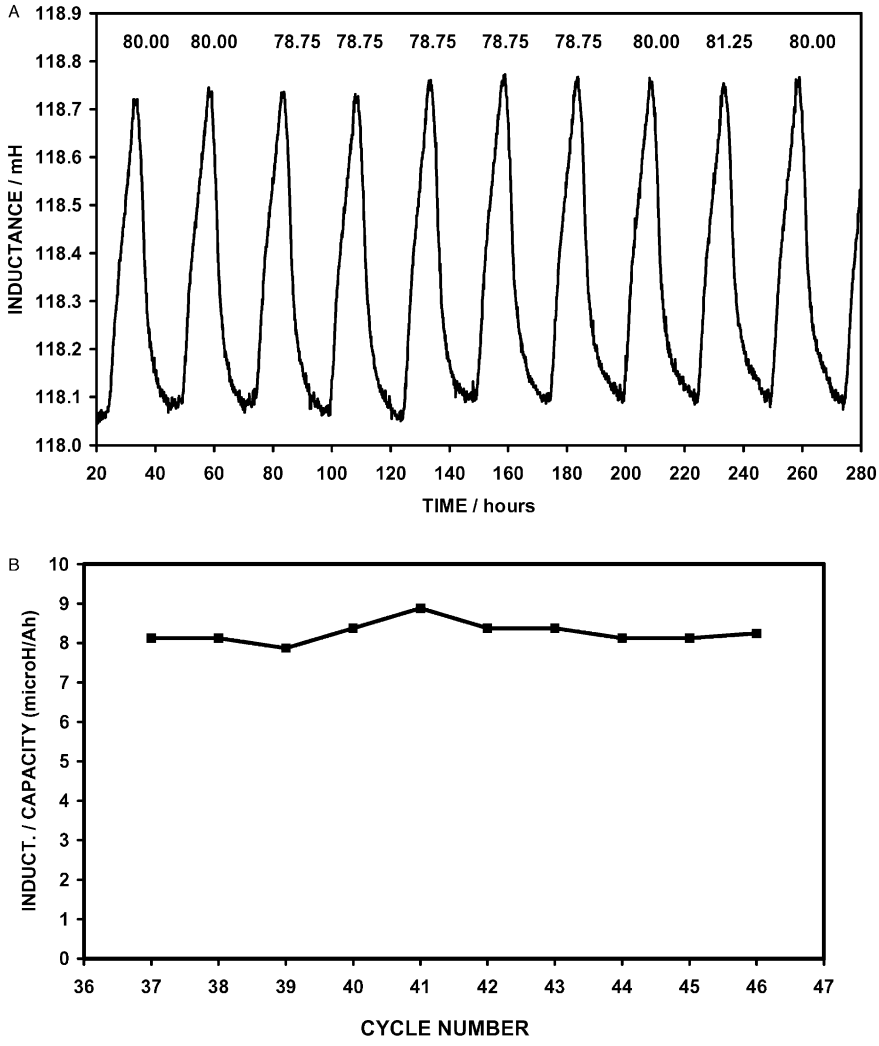

Fig. 4. (A) Inductance profiles (10 kHz) for cycles 37–46 of a 6TL battery. The ampere-hour discharge capacities are included above the profiles (9 A discharging, 25 A/14.4 V/14 h charging); (B) Plot of the ratio (inductance change during discharging)/(capacity) for the same cycles.

3.5. Change in shape of the inductance profile for discharging

A closer look at the inductance plots for discharging, in Figs. 4A and 5A, reveals that the discharging portions of the plots are no longer as straight as in early cycles. This change began to be visible around the cycle 20 and is displayed in Fig. 6A, where the cycles 15 and 30 are compared (the background signals at the beginning of discharging were slightly different but have been superimposed for ease of comparison). The change in inductance during discharging decreased from the cycles 15 to 30, whilst the capacity also decreased from 91.5 to 78.75 Ah, because of insufficient charging. In the cycle 30 discharge, the inductance increases more rapidly for about the first half of the discharge and then noticeably slows down. Fig. 6B is a plot of the same data with the time axis of one curve scaled by the ratio of the two discharge capacities, so that the inductance changes at the same states-of-discharge can be directly compared. Now the plots in the first half of discharging are of the same shape, implying that the same behaviour is occurring during this part of the discharge, whilst a different behaviour is seen for the second half. There appears to be an abrupt change in slope, rather than a continuous curve. When the battery was left at open circuit for 2 days after charging, the same shape inductance profile was obtained from discharging, so the changes are from a stable electrode structure. In both Fig. 6A and B, the inductance of the cycle 30 can be seen to be changing less rapidly in the second half of the discharge. This behaviour was found to be dependent on the frequency of the magnetic field, which will be discussed in the next section.

Fig. 7A compares the inductance change of the discharges in the cycles 30 and 110, where the time axis has again been scaled to compare inductance changes at the same states-of-charge. Here, it is seen that the rate of change of inductance near the beginning of discharging has increased for cycle 110, while the shape of the curve for the rest of the discharge

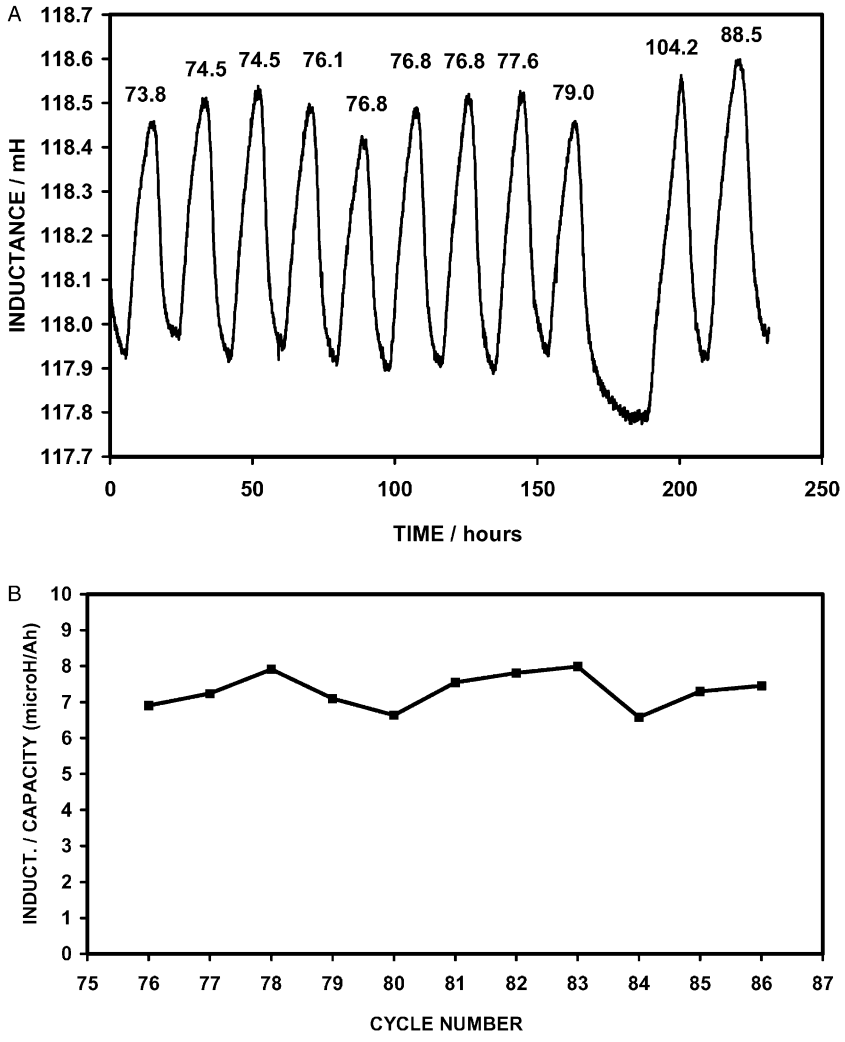

Fig. 5. (A) Inductance profiles (10 kHz) for cycles 76–86 of a 6TL battery, using the same cycling regime as in Fig. 4, except that charging time was reduced to 8 h. For cycle 84, the charging time was extended to 25 h; (B) Plot of the ratio (inductance change during discharging)/(capacity) for the same cycles.

is similar to that in cycle 30. Therefore, during the operating life of the battery, the biggest change in the shape of the inductance plots for discharging occurred between cycles 15 and 30. Further information on this behaviour was also obtained from using different frequencies.

Fig. 7B shows an enlarged plot of the cycles 83 and 84, that were also shown in Fig. 5, in which the discharge capacity was low in the cycle 83 because of undercharging, but was recovered by an extended charging time for the cycle 84. Here, it can be seen that the shape of the inductance profile for discharging has been maintained after extensive charging. This indicates that the shape of the first part of the discharge inductance profile is related to the structure of the electrode and is not associated with passivation. The additional capacity in cycle 84 led to the inductance changing at the same rate, during discharging, as in the later part of cycle 83. Therefore, those parts of the electrode that had been sulphated did not yield a different rate of change of inductance during discharging in cycle 84.

3.6. Frequency dependence

In order to learn more about the change in slope of the inductance plot during discharging, measurements were made at different frequencies. This was because the different skin depths of the magnetic field allowed for a certain degree of depth profiling of the negative electrode. Fig. 8A compares the inductance profiles of cycle 121 of the 6TL lead-acid battery at 1, 3, 10 and 30 kHz. In order to compare the shapes of the curves, all of the backgrounds have been adjusted to that for 10 kHz. Although the inductance change is greatest at 30 kHz, the signal-to-noise ratio of the data is not as good as that at 10 kHz. In fact, the signal was rising in magnitude at 30 kHz because the frequency was approaching the resonance frequency of the pot-core coil, which was 70 kHz. A lower frequency allows sampling to greater depths into the lead electrode, but the detected change in inductance is also lower in magnitude. This is because the eddy currents that are induced by the coil are concentrated,

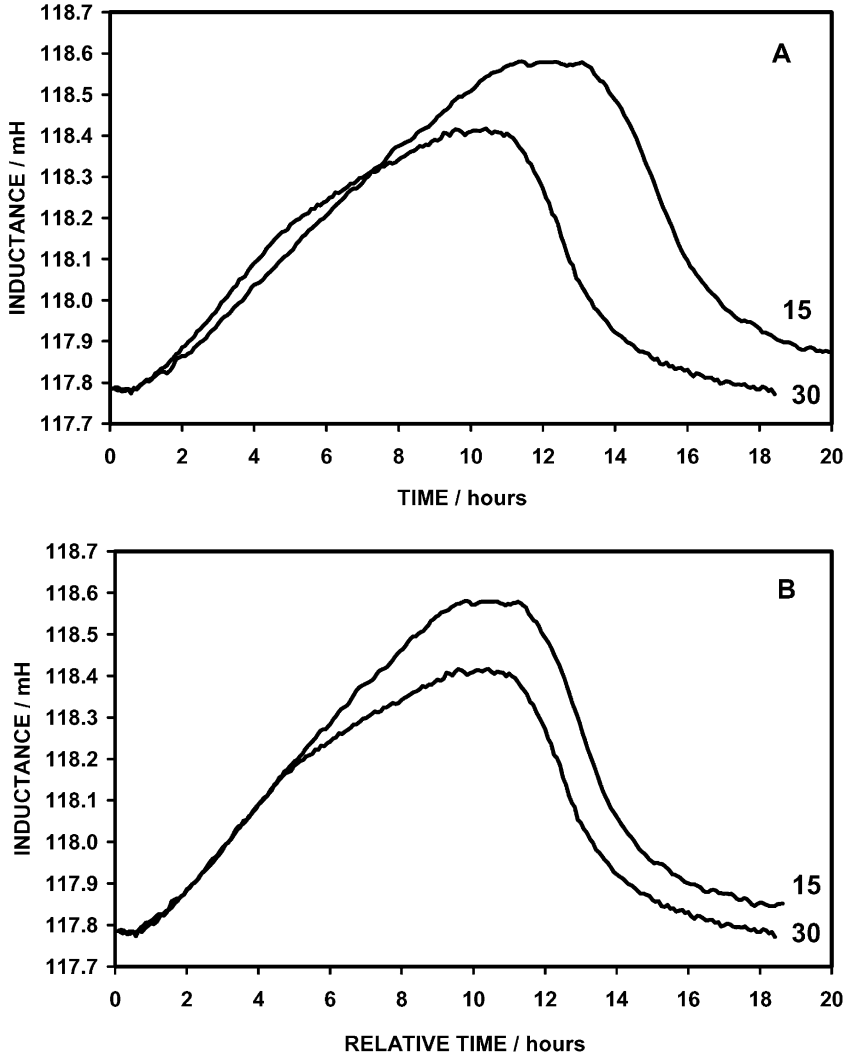

Fig. 6. A comparison of the inductance profiles (10 kHz) of the cycles 15 and 30 of the same 6TL battery, with the background inductance adjusted to the same value: (A) The inductance change during discharging appears to change slope approximately halfway through the 30th discharge; (B) The same data with the time scale of cycle 15 normalised to that of cycle 30, so that the inductance profiles reflect the same states-of-charge.

on average, further away from the coil and, therefore, the secondary magnetic fields associated with those currents do not interact as strongly with the coil. The actual shapes of the inductance plots during the cycle are compared in Fig. 8B. Here, the inductance changes have all been normalised to that at 30 kHz. There are clearly two separate components to the inductance plots during discharging and there is a definite frequency trend. The steeper curve that was obtained during the first half of the discharge is more prominent at lower frequencies. The higher rate of change of inductance at 1 kHz implies that the charge transfer reactions during the first 30–50% of the discharge are concentrated more in that part of the end plate furthest away from the coil. The skin depth is 7.3 mm at 1 kHz, so the magnetic field will be traversing the 2 mm thickness of the end plate. The much smaller slope of the 1 kHz plot during the second half of the discharge, in conjunction with the plots at other frequencies, indicates that the charge transfer reactions now must be occurring closer to the coil, on average.

The behaviour observed in Fig. 8 can be explained in terms of the porous nature of the end plate of the battery, which is the only electrode being sampled. Only one surface of the end plate is facing a positive electrode and that surface is likely to be discharged more quickly because of electrolyte migration effects. The discharge reaction taking place at the negative electrode proceeds via a solution–precipitation mechanism and can be written as [6]:

$$Pb \rightarrow Pb^{2+} + 2e^{-}$$

$$Pb^{2+} + HSO_4^{-} \rightarrow PbSO_4 + H^{+}$$

here, migration and diffusion of the large anions through the micropores of the negative electrode structure is rate determining [7]. At higher discharge rates, reaction will be concentrated towards the surface of the electrode further

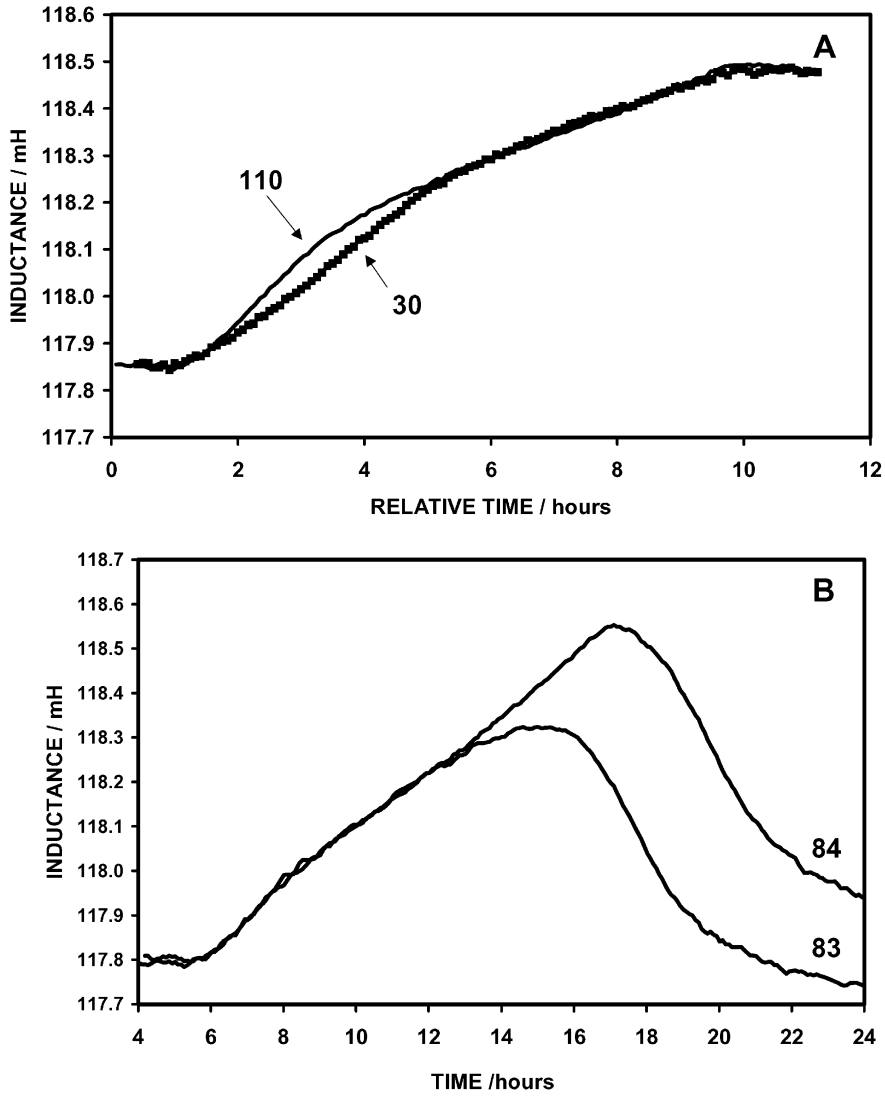

Fig. 7. (A) Comparison of the inductance profiles (10 kHz) of the cycles 30 and 110 for discharging a 6TL battery at 9 A. The time axes have been modified so that the curves reflect the same states-of-charge; (B) Comparison of the inductance plots of cycles 83 and 84, showing the effects of extended charging on cycle 84.

from the coil. For example, at 1 kHz, the change in inductance with initial discharging is much faster than that at 30 kHz, because the magnetic field at 1 kHz is probing the far surface of the electrode, on average, whilst the 30 kHz field is sampling material closer to the coil. The discharging rate being used in these experiments was approximately *C*/10, which would be expected to give a fairly uniform distribution of lead sulphate in the negative electrode, whereas discharging at the *C* rate or higher, would be expected to lead to passivation of the surface of the electrode before the interior of the electrode has been fully oxidised [8,9]. However, the end plate only has a counter electrode on one side but is still of the same thickness as the other negative plates. Therefore, it will inevitably behave differently and will develop a discharge product concentration gradient at lower discharge rates than the other electrodes.

During the first 20–30 cycles of a lead-acid battery, the electrode structures rearrange and become more porous [5]. The large increase in molar volume of the active mass that occurs during discharging must be a driving force for this change. The active material has a primary skeletal structure of lead that supports a secondary structure of crystals of active material that are oxidised and reduced [5]. The skeletal structure of the active material at the surface of the electrode will be weaker than that in the bulk electrode, which may result in a higher concentration of large pores being formed at the surface during these early cycles. Fig. 6B showed that the inductance change near the beginning of discharging for cycles 15 and 30, appeared to arise from the same behaviour and that it is the behaviour obtained during the second half of discharging that is different. Fig. 7B showed that removal of sulphation (due to undercharging) did not change the shape of the inductance profile for short discharge times. If we assume that the sulphation was mainly causing blockage of micropores, then there is the implication that the second part of the inductance profile is associated

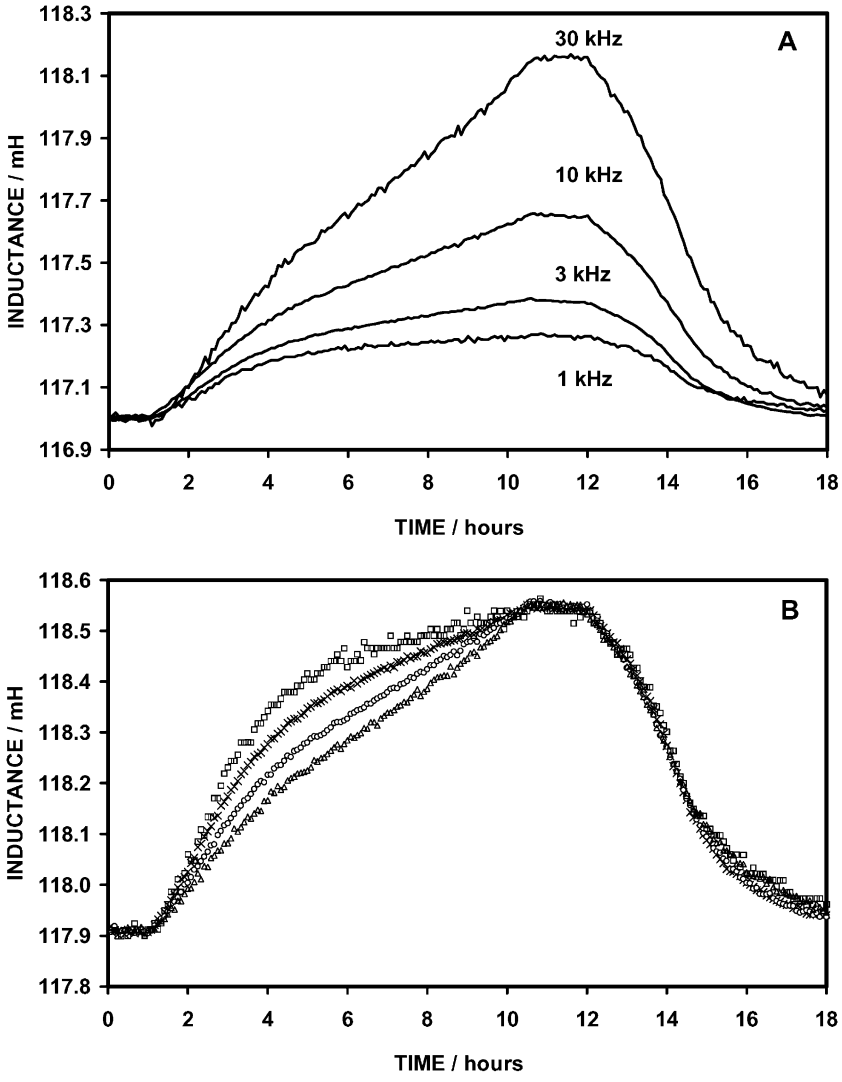

Fig. 8. A comparison of the inductance profiles at 1, 3, 10, and 30 kHz, for the cycle 121 of a 6TL battery (9 A discharging, 25 A/14.4 V/14 h charging): (A) The data have been adjusted to the same background at zero time; (B) The profiles have been normalised to the same maximum in order to compare their shapes ((□) 1 kHz, (×) 3 kHz, (○) 10 kHz, and (△) 30 kHz).

more with small pores than the first part. The walls of large pores will have a greater thickness of lead in the charged state than micropores and, therefore, should support a greater flux of eddy currents. In the absence of further data, we conclude that the discharge reaction is occurring preferentially towards the inward facing surface of the end plate, even at the low rates of discharge used here ($\sim C/10$). The change in slope of the inductance profile may arise because there is a higher concentration of large pores towards the inward-facing surface and that discharging, on average, is concentrated in these pores during the first part of discharging.

3.7. Comparison of charging and discharging inductance profiles

Fig. 9A compares the inductance changes for the cycles 9 and 110, plotted against the total absolute charge passed. It is apparent that the inductance plot for charging has also changed with cycling but, unlike for discharging, the plot has become less curved with time. The inductance profiles for charging and discharging are certainly not of the same shape. The majority of cycling was carried out using a constant current of 9 A for discharging and a maximum charging current of 25 A, so there will be a rate-related difference (see later). The nature of the electrochemical reaction at the negative electrode is important: with discharging, the bulk electrolyte needs to supply large sulphate ions to the negative electrode in order to form the lead sulphate, but with charging, the bulk electrolyte needs to supply hydrogen ions which have much higher mobility. Therefore, the charging reaction should proceed much more uniformly throughout the electrode. Fig. 9B compares the inductance changes at 3 and 10 kHz for the cycle 125. Here the charging profiles are similar, while the discharging profiles are

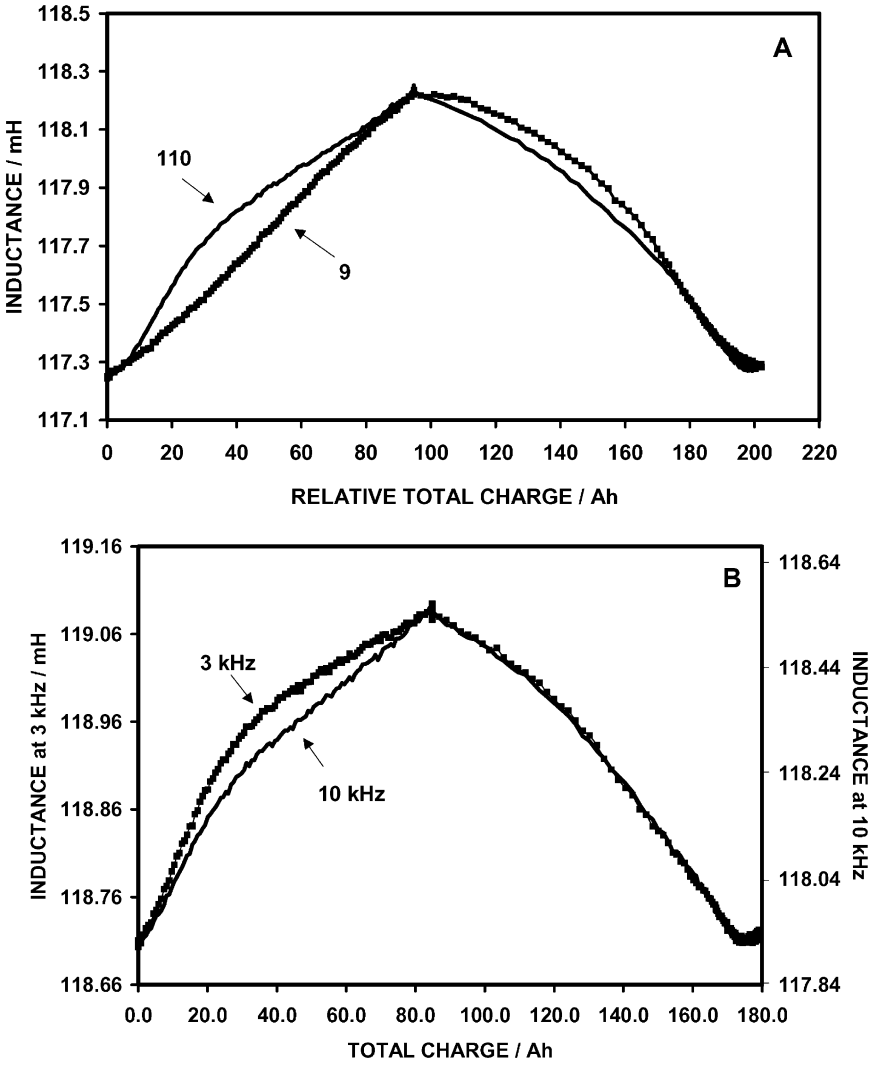

Fig. 9. (A) A comparison of the shape of the inductance profiles (10 kHz) of the cycles 9 and 110 of a 6TL battery, plotted against the total absolute charge passed. The scales have been adjusted to the same capacity; (B) A comparison of the inductance profiles, at 3 and 10 kHz, for cycle 125 of a 6TL battery.

different in agreement with the above supposition (the charging reaction is discussed further, later in this section).

Further cycles were carried out using 10 A and 6 A charging current limits. This did not affect the shape of the inductance profile of the following discharge, although the effect of longer term cycling has not yet been established. The inductance behaviour during charging did change, however, as can be seen in Fig. 10A, where the profile is now almost linear for 10 A charging. Again, it is instructive to attempt to explain the origins of this change. One important factor is the loss of charging current to resistive and polarisation heating. This loss is represented by the difference in the charge passed during charging and discharging. For the 25 A charging cycle shown in Fig. 10A, this difference was 8.66 Ah. Fig. 10B shows the same cycle and includes the temperature change. The inductance curve for charging was corrected for the charge lost to heating effects by making the approximation that the loss of charge was proportional to the temperature rise. Any thermal losses were assumed to be small and were neglected. The corrected curve is also shown in Fig. 10B (black squares), and it is seen to be more curved than the uncorrected one. The plot for 10 A charging would have a smaller correction, because the temperature rise was only 3°C, but it is apparent that the corrected plots for 25 A and 10 A charging do not compare. The correction for the loss of charging current to heat does not have a counterpart for discharging, since the discharge reaction itself is providing the energy.

The difference between the inductance profiles for charging at 10 A and 25 A might, at first thought, be explained in terms of the reaction occurring closer to the electrode surface at the higher current. However, the inductance profiles for charging are similar at all the frequencies employed (Figs. 8B and 9B) and, as we have already stated, the charging reaction is expected to be more uniformly distributed throughout the electrode than the discharge reaction.

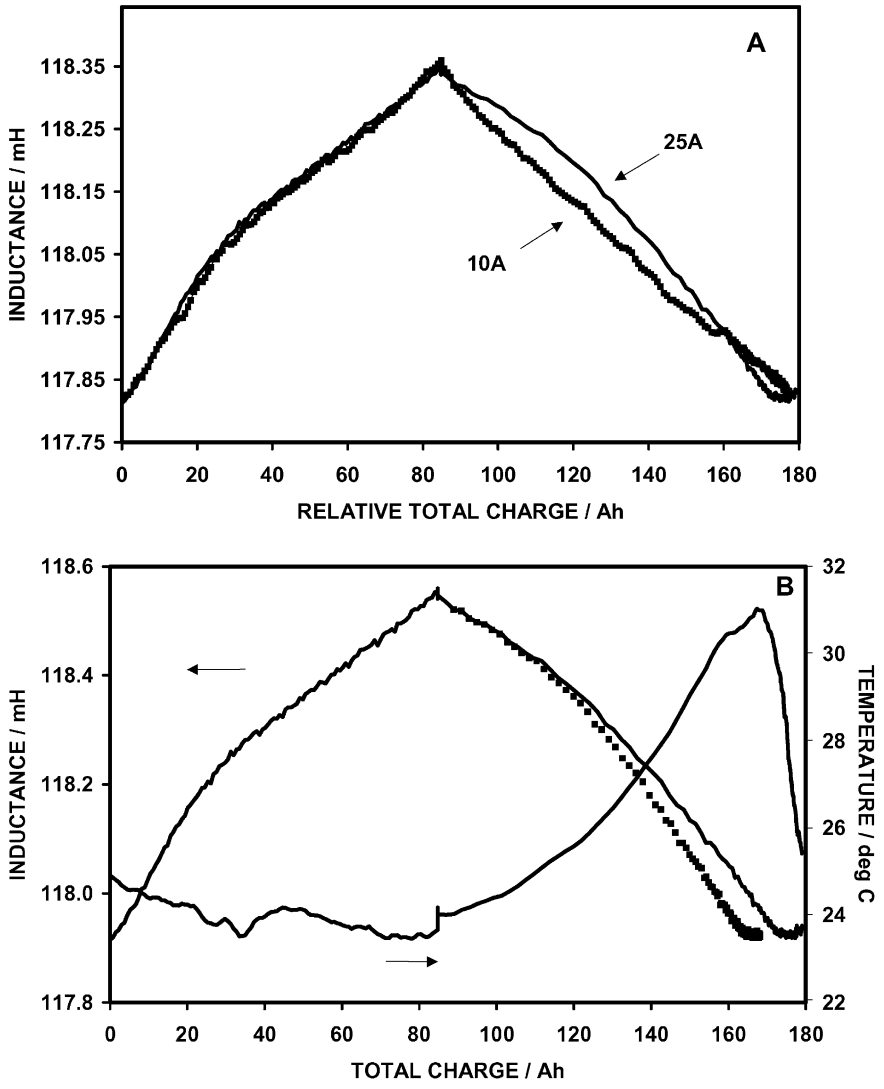

Fig. 10. (A) A comparison of the inductance profiles (10 kHz) for a cycle using 9 A discharging and 25 A/14.4 V/14 h charging, followed by one using 10 A charging; (B) The same 25 A profile as in A, showing the correction for loss of charge to heat during charging.

The reduction of $PbSO_4$ to Pb proceeds via dissolution of $PbSO_4$ and electrochemical reduction of the Pb^{2+} ions at the lead grid interface.

$$PbSO_4 + 2H^+ \rightarrow Pb^{2+} + H_2SO_4$$

$$Pb^{2+} + 2e^- \rightarrow Pb$$

The charging reaction is known to begin at the grid/active material interface [10]. The reaction rate depends upon the real area of the interface between the $PbSO_4$ crystals and the lead grid, and it has been shown that larger crystals contribute less to the overall current because of their smaller reaction site area per unit volume [11]. Given the high transference rate of hydrogen ions and the high exchange current density at the grid interface, the rate-determining step is the dissolution of $PbSO_4$. Therefore, the recharging reaction should proceed uniformly throughout the porous electrode. The smaller frequency dependence of the shape of the charging inductance profile supports this behaviour. The largest $PbSO_4$ crystals will be the last to be fully reduced. The crystals are believed to react from the outside surfaces inwards, with the $PbSO_4$/Pb-grid interface being the last part to be reduced [11]. In this sense, one would expect a larger increase in current flux near the end of charging, when the interface with these large crystals becomes fully conducting. Such behaviour can be seen in Fig. 10A for 25 A charging. However, a very different inductance profile is observed for charging at 10 A, which is almost linear. In order to explain this change, we suggest that the lower charging rate has affected the equilibrium of the reaction such that the dissolution rate of $PbSO_4$ in the larger crystals is now relatively faster. Electrolyte exchange is required in the $PbSO_4$/Pb interfacial region and such exchange will be slower for the larger crystals because the reaction front propagates inside

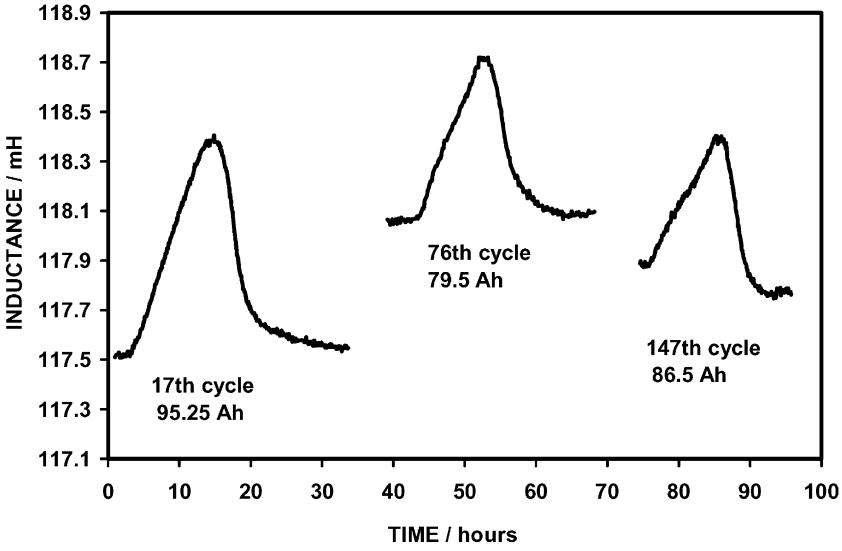

Fig. 11. Inductance profiles (10 kHz) for cycles at different stages of the 6TL battery life.

the crystals. Therefore, these large crystals will have a higher local concentration of H_2SO_4. Because $PbSO_4$ becomes less soluble as the concentration of acid increases, reaction is slower for the larger crystals. It is possible that reducing the charging current to 10 A is sufficient to allow the local concentration of acid in the large crystals to fall and allow the dissolution rate of the $PbSO_4$ to increase close to that of the smaller crystals. Further work is being carried out in order to investigate this possibility.

3.8. State-of-charge monitoring throughout the cycle life

Returning to the question of using inductance to monitor the SOC of a battery, Fig. 11 compares the inductance plots at 10 kHz for the cycles 17, 76 and 147 of the same 6TL battery. The inductance plot for discharging was still almost linear for the cycle 17 and the background was still increasing. Although the background signal varied significantly during the cycle life, the inductance change during a given discharge was fairly constant but tended to fall in magnitude with battery aging. For example, let us take the ratio of (inductance change)/(capacity) for the discharge of the cycle 17 and normalise this to 1.0. Then the ratios compare as 1.00:0.91:0.65 for the cycles 17, 76 and 147, respectively. Therefore, the magnitude of the change in eddy current flux decreases, for the same discharge rate, as the battery ages. This is not unreasonable because degradation of the active material, in particular islands of lead and passive lead sulphate, will lead to an increased resistance to the eddy currents. Eddy currents can be expected to be affected more by electrode degradation than the discharge capacity is, because of the long current paths of the eddy currents in comparison with the maximum possible distance between the grid and the active material. Fig. 11 shows that the long-term accuracy of these inductance measurements is only acceptable if periodic recalibration is carried out.

4. Conclusions

Measurement of the inductance of wire-wound coils, using ac current in the frequency range of 1–40 kHz, was found to have great potential for non-intrusively monitoring the SOC of lead-acid batteries. The battery–coil combination needs to be calibrated by performing complete discharge cycles and the inductance signal needs to be corrected for temperature variations within the battery. The signal from fresh batteries tends to drift upwards during the first 20–30 cycles while the negative electrodes restructure. The inductance profile for discharging changed in shape at the same time, so the whole of the inductance profile is needed for SOC estimation. There is a hysteresis in the inductance profiles for charging and discharging, so separate calibration curves are needed to follow charging. The inductance signal needs to be recalibrated approximately every 10 cycles in order to maintain accuracy. The accuracy of the technique is estimated at $\pm 10\%$ for randomly measuring the SOC during 10 cycles following calibration, falling to $\pm 7\%$ if the inductance is known at the beginning of the discharge in question. For cycles that include significant undercharging these figures may increase to ± 20 and $\pm 12\%$. This technique should be particularly useful for monitoring the SOC of sealed or gelled-electrolyte lead-acid batteries and for identifying the end-of-charge of the negative electrode.

The use of different frequencies showed that discharging was not uniform in the end plate, but was initially occurring close to the inward facing electrode surface (facing the positive electrode). Therefore, the observed signal is not

likely to be the same as that obtained from the other electrodes in the same cell, although this is not believed to be a problem for determining the SOC. The inductance profiles for charging indicated that reaction was uniform with depth into the electrode, at different currents, but that large crystals of lead sulphate are probably affecting the shape of the inductance profile. The magnitude of the eddy currents apparently decreases with long term cycling as the negative electrode active material degrades, and at a faster rate than the capacity.

Acknowledgements

The authors would like to thank Raymond Dore for writing some of the computer programmes used in this work and Brian Lapine for helpful discussions.

References

[1] P.R. Stevenson, US Patent no. 5,093,624 (1992).
[2] D. Limuti, J.M. Ross, T.L. Churchill, US Patent no. 5,132,626 (1992).
[3] J.F. Beutler, B.J. Burreson, W.A. van Schalkwijk, D.F. Flagg, G.A. Kromholtz, J.J. Green, US Patent no. 5,537,042 (1996).
[4] E.Y. Weissman, in: K.V. Kordesch (Ed.), Batteries, Vol. 2, Marcel Dekker, New York, 1977 (Chapter 1).
[5] D. Pavlov, E. Bashtavelova, V. Iliev, in: Proceedings of a Symposium on Advances in Lead Acid Batteries, The Electrochemical Society, Pennington, NJ, USA, 1984, p. 16.
[6] P. Ekdunge, D. Simonsson, J. Appl. Electrochem. 19 (1989) 127.
[7] Y. Guo, J. Electrochem. Soc. 142 (1995) 3643.
[8] M. Barak, in: M. Barak (Ed.), Electrochemical Power Sources, IEE, London, UK, 1980 (Chapter 4).
[9] K. Asai, M. Tsubota, K. Yonezu, K. Ando, Power Sources 10 (1984) 481.
[10] M.A. Dasoyan, I.A. Aguf, in: Current Theory of Lead Acid Batteries, ILZRO, New York, 1979 (Chapter 5).
[11] Z. Takehara, J. Power Sources 85 (2000) 29.